This article has been accepted for publication in IEEE Open Access Journal of Power and Energy. This is the author's version which has not been fully edited and content may change prior to final publication. Citation information: DOI 10.1109/OAJPE.2026.3666226

A Measurement-Driven Digital-Twin Methodology for Flexible Loads Voltage Control in Unknown Grids

JESÚS ARAÚZ[†*], ANTOINE LABONNE[*], YVON BESANGER[*], *Senior Member, IEEE*, FRÉDERIC WURTZ[*], *Member, IEEE*, SIMON WACZOWICZ[†], VEIT HAGENMEYER[†], *Member, IEEE*

[1] Univ. Grenoble Alpes, CNRS, Grenoble INP, G2Elab, Grenoble, 38000, France
[2] Karlsruhe Institute of Technology, Institute for Automation and Applied Informatics, Kaiserstraße 12, Karlsruhe, 76131, Germany

CORRESPONDING AUTHOR: Jesús Araúz (e-mail: jesus.sarmiento@kit.edu).

This research was partly funded by the IRGA Foundation of Université Grenoble Alpes, by the French National Research Agency in the framework of the "Investissements d'avenir" program (ANR-15-IDEX-02), and the Helmholtz Association of German Research Centres (HGF) within the framework of the Program-Oriented Funding POF IV in the program Energy Systems Design (ESD, project numbers 37.12.01, 37.12.02, and 37.12.03).

ABSTRACT

Voltage control in modern power systems has become increasingly complex due to the high penetration of renewable generation. Numerous solutions have been proposed from both the transmission and distribution sides, involving generators and system operators. However, the contribution of loads has remained limited, mainly to demand shifting and basic demand response strategies. This work introduces a novel approach that leverages digital twins to enhance the active participation of loads in supporting voltage control. Unlike traditional methods, the proposed framework builds digital twins exclusively from measurable data, enabling virtually any converter-interfaced load connected to a grid, regardless of whether the network is fully known or not, to contribute effectively to voltage regulation. The methodology is first demonstrated through a parametric study, which evaluates the impact of different load behaviors and control strategies on network voltage stability. To further validate the approach, hardware-in-the-loop (HIL) experiments are conducted, confirming the feasibility of real-time implementation. Four voltage control use-cases are developed and tested for a controllable thermal load, showing that even individual loads can provide meaningful support to grid voltage regulation. The results highlight the potential of data-driven digital twins to unlock new, scalable, and flexible contributions from loads, reinforcing the stability of future power systems with high renewable penetration.

INDEX TERMS Demand response, Digital Twins, Voltage control, Hardware-in-the-Loop, Machine learning, Methodology, Thermal loads.

I. INTRODUCTION

Mitigating climate change requires a deep transformation of the energy sector, including tripling renewable capacity and improving efficiency by 2030 [1]. Large-scale integration of renewable generation (RG) advances decarbonization but poses two main challenges [2]: achieving a cost-effective supply–demand balance and ensuring grid security with high shares of converter-interfaced generation (CIG) [3]. Addressing these challenges demands further research on converter technologies, control strategies, and their grid integration.

The increasing share of CIG introduces new challenges to power systems. Traditional dynamics are being reshaped by the variability of renewable sources such as wind turbines (WT) and photovoltaic (PV) plants, along with the widespread use of power electronic devices [4]. These devices are embedded not only in CIG, but also in modern loads, energy storage systems (ESS) [5], and transmission equipment, making it necessary to redefine power system stability concepts [6].

Voltage stability has become one of the most critical issues under these conditions. The integration of non-dispatchable renewable generation and distributed storage in active distribution networks is creating new challenges for real-time voltage regulation. Traditional voltage control schemes were not designed to handle the dynamics imposed by high penetration of power electronics, and may therefore limit the

This work is licensed under a Creative Commons Attribution 4.0 License. For more information, see https://creativecommons.org/licenses/by/4.0/

Nomenclature

Acronyms

AI	Artificial Intelligence
CIG	Converter-interfaced generation
CILs	Converter-interfaced loads
DR	Demand response
DT	Digital twin
ESS	Energy storage systems
EV	Electric Vehicle
FACTS	Flexible AC transmission systems
FIDVR	Fault-induced delayed voltage recovery
HIL	Hardware-in-the-Loop
HVAC	Heating, ventilation, and air conditioning
LR	Linear regression
ML	Machine learning
MPC	Model predictive control
OPF	Optimal Power Flow
PMUs	Phasor Measurement Units
PV	Photovoltaic
RG	Renewable generation
RMS	Root mean square
SST	Solid-state transformers
STATCOMs	Static Synchronous Compensators
SVCs	Static Var Compensators
WT	Wind turbine

Parameters

η	HVAC system efficiency
A_{ji}	Heat transfer area related to i^{th} and j^{th} thermal systems in m^2
C_i	Thermal capacity of the i^{th} thermal system in kJ/ °C
$C_{1,2,3}$	Linear regression coefficients in V, V/W, and V/W^2, respectively
n	Number of unknown loads
Per_{unk}	Oscillation period of the unknown load in s
R_{eq}	Equivalent balanced grid resistance in Ohms
U_{ji}	Heat transfer coefficient related to i^{th} and j^{th} thermal systems in $kW/m^2/$°C
X_{eq}	Equivalent balanced grid reactance in Ohms
sh	Phase shift in boolean

Subscripts

i	i^{th} thermal subsystem
j	j^{th} thermal subsystem
base	base
ctrl	control
eq	equivalent
grid	grid
imag	imaginary
inj	injected
max	maximum
mid	average
min	minimum
mtr	motor
net	net
NoCtrl	without control
P-to-ω	Power to angular speed
real	real
set	setpoint
unk	unknown
zone	zone

Variables

$\dot{m}$	HVAC system mass flow in Kg/s
ω_{mtr}	angular speed in rad/s
$\underline{I}$	Line current in A
E_{grid}	Equivalent balanced grid voltage in V
P_{ctrl}	Controllable load active power in W
P_{net}	Load active power in W
P_{NoCtrl}	Uncontrollable part of the load active power in W
$P_{\text{unk}}(t)$	Time-dependent unknown active power in W
P_{HVAC}	HVAC system electric power in kW
Q_{net}	Load reactive power in VAR
Q_j	j^{th} heat gain in kW
Q_{HVAC}	HVAC system heat gain in kW
$r_{\text{P-to-}\omega}$	Power to angular speed ratio in W/(rad/s)^3
t	Time in s
T_i	i^{th} thermal system temperature in °C
T_j	j^{th} thermal system temperature in °C
T_{inj}	Injected air temperature in °C
T_{set}	Setpoint temperature in °C
T_{zone}	zone temperature in °C
V_{imag}	Imaginary component of the equivalent balanced load node voltage in V
V_{real}	Real component of the equivalent balanced load node voltage in V
V_{set}	Setpoint voltage in V

adoption of renewable energy resources in the future grid if not properly addressed [7]. The development of real-time voltage control schemes that exploit the capabilities of RG is essential to mitigate grid stability problems and to support the transition to 100% renewable-based consumption.

II. STATE OF THE ART

Traditional control schemes are often insufficient to address new challenges. Grids are increasingly vulnerable to voltage fluctuations, cascading trips, and phenomena such as Fault-Induced Delayed Voltage Recovery (FIDVR), especially in systems with many induction motor loads. In distribution grids, additional issues arise from distributed RG, including PV-induced overvoltage at low-voltage feeders, voltage drops from electric vehicle (EV) charging, and reversed power flows that challenge line voltage regulators. Coupling between transmission and distribution operators also increases coordination needs to ensure secure operation [8].

Advanced voltage control strategies, including novel means of provision such as solid-state transformers (SST) [9], are therefore essential. Conventional reactive compensation devices (e.g., capacitor banks, Static Var Compensators (SVCs), and Static Synchronous Compensators (STATCOMs) remain vital for fast regulation but are more effective when combined with optimal placement, sizing, and coordination. Distributed RG inverters provide dynamic active and reactive power support to reduce variability. Hierarchical and model predictive control (MPC) improve multi-time-scale coordination, while adaptive droop controllers enable smart inverters to adjust to varying conditions. Demand Response (DR) programs [10] further help alleviate peak stress and limit violations [7], [11].

The evolution of voltage control is increasingly linked to digitalization and data-driven methods. Measurement-based approaches using Phasor Measurement Units (PMUs) and real-time digital simulators provide high-resolution monitoring and fast response capabilities [7]. At the same time, artificial intelligence (AI) and machine learning (ML) methods are enabling predictive, adaptive, and distributed control solutions that enhance resilience against RG uncertainties [8]. Voltage stability can be strengthened by synergies between ESS, flexible AC transmission systems (FACTS), and grid modernization initiatives [12].

Most traditional and emerging proposals to improve voltage control in grids are designed for generators and auxiliary components (i.e., FACTS) [7], [8], [11], [12]. Approaching global objectives [1] directly implies an increase in smart and sustainable consumption. Grid-responsive loads may reduce the extension of ancillary services provided by generation [13], [14].

Recently, converter-interfaced loads (CILs) have been widely considered to provide distributed frequency control [15]–[18], mainly thermal loads such as refrigerators and heating, ventilation, and air conditioning (HVAC) systems. These loads may easily leverage the basis of advanced control proposals (e.g., distributed approach, data-driven, AI/ML-based, etc.) by adapting their controllers. Additionally, an emerging concept that integrates these characteristics is the Digital Twin (DT) [19]. As evidenced in [20], DTs are growing for frequency control provision, although most works do not implement the self-update capacity, i.e., the ability of the DT to adapt and reconfigure itself to mirror changes in the physical asset.

A few works have proposed the use of DT for enhancing voltage performance. In [21], a spatio-temporal graph DT is proposed to improve the computing time and accuracy of the state estimation. Although it is not voltage control, it can be extended to this service. In [22], a DT is proposed to ensure the resilience and voltage levels of space-based power systems under faults. In [23], an optimal power flow (OPF) is performed in a DT of the grid to improve the voltage performance. Similarly, in [24], the capacitor banks and transformer taps are also included in the OPF, in addition to the RG. Some authors do not explicitly mention DT, but still create AI/ML-based grid models to improve voltage control [25], [26].

Research on responsive loads enabled by DTs is even more limited. In [27], a grid DT is developed to monitor voltage stability and system performance, thereby determining the optimal load shedding strategy. Although not explicitly framed as a DT, [28] applies AI techniques for load forecasting and DR, where voltage regulation is achieved through load curtailment.

Currently, DTs have been mainly proposed for the operation, management, and control of energy assets; maintenance and fault diagnosis; energy management; system optimization and resource allocation; cybersecurity; planning and disaster response; and stability assessment and enhancement, including voltage control; among other uses [29]–[31].

As noticed, the implementation of DTs in CILs for the provision of ancillary services is underexplored. Some authors have proposed DTs to update the load consumption [27], [28]. However, load consumption is not considered to be constantly updated; load intrinsic dynamics is not considered; the DT of the grid does not show its self-update capability; and the DT quality depends on high-complexity AI/ML techniques, high-memory availability, and extensive measurements.

Addressing the identified gap, this work proposes a methodology for using grid DTs to enhance the contribution of locally controllable distributed loads to voltage control, covering both steady-state and slow dynamics. The main contributions are summarized as follows:

- Highlighting the limited attention given to load-based voltage control and the absence of DT-oriented DR strategies.
- Introducing a self-adaptive grid DT that updates online to provide local system awareness.
- Presenting an ML-based procedure to construct and refresh the DT, suitable for partially unknown grids.

- Introducing representative DT-enabled control logics to illustrate how the proposed methodology can be applied.
- Validating the practical feasibility of the framework through dual-HIL experiments on an HVAC system with coupled electrical and thermal dynamics.

The remainder of the paper is structured as follows: Section III presents the methodology for creating the DT, load, and voltage control. Section IV includes the parametric study and real-time validation of the DT, as well as the real-time experimental validation of the voltage control. Section V states the findings, conclusions, limitations, and future works.

III. METHODS

Implementing a voltage control-oriented DT requires the model of the grid to be supported, as well as the load and possible voltage control schemes. As noticed in Section II, extensive information is required for an accurate model. The present work focuses on enabling nearly any controllable load to provide voltage control in unknown grids, where having access to feeders and other load data is not possible or realistic.

A. Grid Digital-Twin

Grids at the transmission or distribution [32] level can be modeled in numerous ways [33]. For voltage phenomenon studies, it is common to implement Kirchhoff's laws, where feeders are described as impedances, and generation and consumption as power flows. From the perspective of a load connected to any grid node, a simple two-bus model can be analyzed [31]:

$$\begin{aligned} &E_{\text{grid}} = (R_{\text{eq}} + jX_{\text{eq}})\,\underline{I} + (V_{\text{real}} + jV_{\text{imag}}) \\ &\text{where} \quad \underline{I} = \left(\frac{P_{\text{net}} + jQ_{\text{net}}}{V_{\text{real}} + jV_{\text{imag}}}\right)^{*} \end{aligned} \tag{1}$$

Equation (1) describes the equivalent balanced grid with voltage E_{grid}, resistance R_{eq}, and reactance X_{eq}. The subscript "eq" refers to the equivalent grid (e.g., Thévenin equivalent) as perceived at the load terminals, providing a generalized representation of any underlying network. The controllable load connection point voltage is described by its real and imaginary components, V_{real} and V_{imag}, respectively. The current, $\underline{I}$, is defined by the net active and reactive powers, P_{net}, and Q_{net}, respectively. Equation (2) is obtained by solving (1) for V_{real} and V_{imag}.

$$\begin{aligned} &(V_{\text{real}})^2 - E_{\text{grid}}V_{\text{real}} + R_{\text{eq}}P_{\text{net}} + X_{\text{eq}}Q_{\text{net}} + (V_{\text{imag}})^2 = 0 \\ &\text{where} \quad V_{\text{imag}} = \frac{R_{\text{eq}}Q_{\text{net}} - X_{\text{eq}}P_{\text{net}}}{E_{\text{grid}}} \end{aligned} \tag{2}$$

As observed, V_{real} can be obtained through a quadratic solution. Together with V_{imag}, both the amplitude and the angle can be readily determined. However, complete information about the impedance of each grid element, as well as the power of every load and generator, is required. In practice, any load connected to the grid, ranging from factories to household appliances, is unlikely to have access to such data.

By considering the superposition principle from basic circuit theory and the well-known relation between voltage and active power [12], it is possible to solve (2) by only accounting for the controllable load of interest, while treating the impact of other loads and generators as noise. Equation (3) presents the general formulation of the DT within a physics-inspired, data-driven framework.

$$|V| = f(P_{\text{ctrl}}) \approx C_1 + C_2 P_{\text{ctrl}} + C_3 (P_{\text{ctrl}})^2 \tag{3}$$

In (3), $|V|$ denotes the measured voltage magnitude at the load connection node, and P_{ctrl} is the measured controllable-load active power. These two quantities constitute the input measurements used to identify the DT. The output of the identification process is the regression model characterized by the coefficients C_1, C_2, and C_3, obtained through linear regression (LR). As discussed in [20], multiple approaches may be adopted depending on the specific requirements. Here, (3) is used solely to show a possible implementation of the proposed digital-twin methodology, rather than to benchmark numerous techniques. A comparative assessment of these techniques is beyond the scope of the present work.

It is important to note that the precision of the proposed linear approximation, commonly described by R^2 [34], strongly depends on the influence of neglected variables (i.e., the power of other consumers/producers, including reactive power) at the time the measurements are collected for LR. Consequently, the probing signal developed by the controllable load should be operated to sufficiently and appropriately excite the system while respecting this constraint [20], [35].

It should be noted that (3) does not aim to represent the full "Voltage–Active Power" relationship, but rather the local voltage sensitivity to the controllable load, which can vary over time. For this reason, the DT is updated online by collecting recent voltage and probing-signal measurements and recomputing the LR model whenever user-defined triggering conditions are met. These conditions may depend on implementation-specific thresholds, such as clock-based refresh, voltage deviations, voltage-to-power ratio changes, load variations, unacceptable R^2, or detected abnormalities, thereby enabling continuous adaptation of the DT to the evolving grid state.

In addition, to ensure low memory usage and reduced computational cost, a linear regression with a single control variable is adopted. In practice, it is usually more feasible to adjust the active power consumption of loads through their current controls than to modify their reactive power [17]. For this, both signals, $|V|$ and P_{ctrl}, are commonly accessible without the need for additional devices.

B. Controllable load modeling

Depending on the specific study, the dynamics involved, and the hypotheses under investigation, loads can be represented using different modeling approaches [20], [36]. As detailed in [17], the compressor/fan/pump-motor assembly of controllable loads, such as HVAC systems and refrigerators, is typically driven through a series connection comprising a rectifier (single- or three-phase, often with a rheostatic brake) followed by a DC/AC or DC/DC converter, depending on the type of machine. Commonly, the assembly setpoint speed comes from an outer control loop that follows a thermal setpoint (e.g., temperature, mass flow, etc.).

1) Thermal load modeling

Thermal loads represent one of the most heterogeneous, relevant, and rapidly growing categories of demand in power systems, encompassing applications such as HVAC equipment, refrigeration units, and district heating networks [20]. Owing to their flexibility and ubiquity, they are increasingly regarded as suitable resources for the provision of various grid services. The scientific literature already contains a broad body of work addressing their modeling, control strategies, and contribution to ancillary services [13]–[18], [20]. From a practical implementation standpoint, these models are generally structured into two interacting subsystems: the thermal zone to be regulated and the device or system that enforces the control action (4). The thermal behavior of the zone can be represented through a one-dimensional lumped parameter formulation, applied to a collection of k subsystems (walls, roof, floor, etc.). Thereby, C_i denotes the thermal capacity, determined mainly by the mass and specific heat of the i^{th} subsystem, while T_i and T_j represent the respective temperatures of the subsystems i and j. The term $U_{\text{ji}}A_{\text{ji}}$ corresponds to the product of the heat transfer coefficient and the effective area between subsystems i and j, and $\dot{Q}_j$ accounts for the j^{th} heat input among l possible gains (e.g., heat infiltration, solar radiation through windows, internal occupancy).

Additionally, $\dot{Q}_{\text{HVAC}}$ denotes the heat extracted by the HVAC system. As discussed in [20], a variety of HVAC modeling approaches can be considered. In general, the system dynamics are governed by parameters such as mass flow rates $\dot{m}$ (both refrigerant and air), setpoint temperature T_{set}, supply air temperature T_{inj}, zone temperature, and the rotational speed of fan and pump motors ω_{mtr}, among other possible variables. Equation (4) can be extended to incorporate time-varying characteristics, higher-order dynamics, and system-specific constraints as needed.

$$\frac{1}{C_i}\frac{dT_i}{dt} = \sum_{j=1}^{k} U_{\text{ji}}A_{\text{ji}}\left(T_j - T_i\right) + \sum_{j=1}^{l}\dot{Q}_j - \dot{Q}_{\text{HVAC}}$$
$$\text{where} \quad \dot{Q}_{\text{HVAC}} = \eta P_{\text{HVAC}} = f\left(\dot{m}, T_{\text{set}}, T_{\text{inj}}, T_{\text{zone}}, \omega_{\text{mtr}}\right) \tag{4}$$

2) Demand response voltage control

In Section II, various approaches have been proposed to design control loops. In the context of responsive HVAC systems, some works focus on modifying the temperature setpoint [13]–[16], the power setpoint [17], [18], or the mass flow in thermal circuits [20]. Depending on hardware accessibility, adjusting or redefining the power setpoint is often considered a more reliable solution [17].

Beyond the chosen setpoint modification strategy, the DT model in (3) can be employed to optimize controller tuning, predict system behavior, and constrain or scale control actions, among other applications. Equation (5) introduces five low-computational-cost, easy-to-implement voltage control schemes to determine the controllable load power setpoint, P_{set}. As mentioned in Section III-A, the low-complexity nature of the control schemes is intended to ensure their implementability across a wide range of controllable loads. In this context, V denotes the load voltage, V_{set} the voltage setpoint, V_{base} the base voltage, V_{mid} the average voltage, P_{NoCtrl} the fraction of load power not subject to control, and the subscript "at (3)" indicates that the variable is evaluated according to (3).

$$P_{\text{set}} = \begin{cases} P_{\text{ctrl}}\left(V_{\text{at (3)}} \approx \frac{V_{\text{set}}}{V_{\text{base}}} V_{\text{mid at (3)}}\right) & \text{Mode A} \\ P_{\text{ctrl}}\left(V_{\text{at (3)}} \approx V_{\text{set}}\right) & \text{Mode B} \\ P_{\text{NoCtrl}} + \left(V(t) > V_{\text{set}}\right) \left|P_{\text{ctrl}}(V(t)) - P_{\text{ctrl}}(V_{\text{set}})\right| & \text{Mode C} \\ P_{\text{NoCtrl}} + \left(V(t) - V_{\text{set}}\right)\left|\frac{P_{\max}-P_{\min}}{V_{\min}-V_{\max}}\right|_{\text{at (3)}} & \text{Mode D} \\ P_{\text{NoCtrl}} + \left(V(t) - V_{\text{set}}\right)\frac{|P_{\max}-P_{\min}|_{\text{at (3)}}}{|V_{\min}-V_{\max}|} & \text{Mode E} \end{cases} \tag{5}$$

Modes A and B determine the closest power value associated with the setpoint voltage, with Mode A additionally scaling the voltage reference to remain within the feasible range. Modes C, D, and E adjust the required power to satisfy the voltage setpoint. Specifically, Mode C follows the characteristic defined in (3), while Modes D and E implement droop-based strategies. It should be noted that the droop coefficients and operating limits in Modes D and E are directly derived from the same power and voltage extrema used by the DT (i.e., the values indicated with the subscript "at (3)"). As a result, all five control modes operate under the same constraints and admissible ranges, ensuring a consistent and fair comparison across strategies.

Figure 1 presents a generalized interaction scheme between the grid and a controllable load, together with the dual-HIL validation framework. This diagram is not limited to a specific application. It applies to both the HVAC system and to any demand-response-oriented controllable load, mainly those with controllable motors. The structure follows the holistic validation approach introduced in [20], and is consistent with the testing concepts in [37] and the discussions in [38]. A co-simulation between Typhoon HIL and OpenDSS [39] enables real-time grid representation while allowing any load model, implemented in a second

HIL device, to be interfaced with a selected grid node. Continuous arrows indicate the standard exchange of signals between the two HIL platforms.

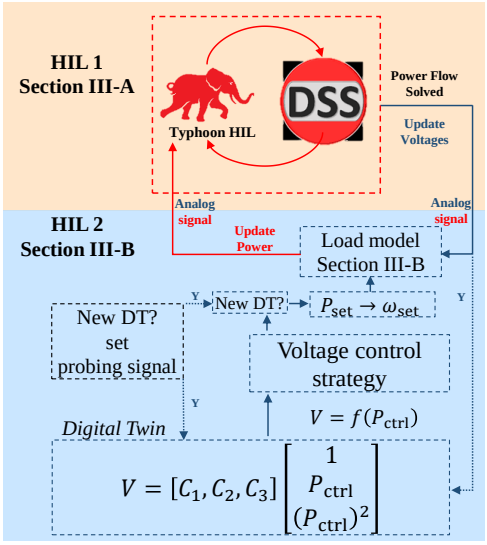

FIGURE 1. Generalized concept and modeling scheme with dual-HIL validation. HIL 1 - Orange: power system side. HIL 2 - Blue: load side. Arrow colors denote the signal target zone. Dashed arrows with "Y" (from "Yes") represent the enabled data flow for DT update when required.

IV. DIGITAL TWIN VALIDATION, IMPLEMENTATION AND APPLICATION

For implementing and evaluating the DT, along with its use for voltage control, computational simulations in Section IV-A, and real-time experimental tests in Sections IV-B and IV-C are carried out. The grid model (i.e., OpenDSS, Simulink, and Co-Sim) is adapted from [40] and accessible at [41], a highly reconfigurable reduced-scale (20 to 0.4 kV, and 30 to 0.03 MW) 14-node distribution grid. Fig. 2 shows the grid under study adapted for dual-HIL validation. For Sections IV-B and IV-C, one thermal load model is adapted from [20]. The model of a space vector PWM voltage source inverter induction motor drive [42] in Matlab/Simulink 2018b is used for the electrical part of the HVAC system. The assembly's rated power is scaled to the rated power of the 9th node, to which the controllable load is connected, while all other nodes, lines, and devices remain as in the base case of [40].

Based on Figure 1, the HIL 1, Typhoon HIL 402, hosts the grid model (solved every 250 ms in OpenDSS by Co-Simulation approach [39]). The HIL 2, OPAL-RT OP5700, hosts the load model (solved every 20 μs) and the grid DT (both built in Matlab/Simulink/RT-Lab). Figure 3 shows the utilized testbench for the tests of Sections IV-B and IV-C. To properly emulate the continuous-time stochastic interaction between any commercial controller, a controllable load, and the surrounding power system, analog I/O signals, sampled at a 100-µs rate and with amplitudes of up to 10 V, are exchanged asynchronously.

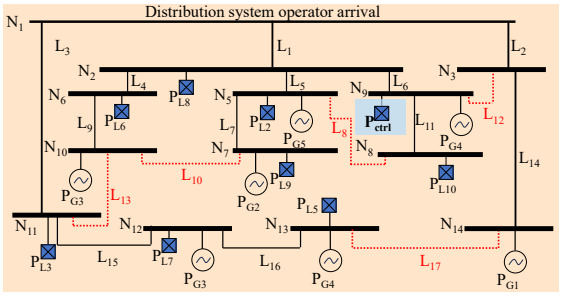

FIGURE 2. Distribution grid under study. N_{1-14} denotes the grid nodes. L_{1-17} denotes the connection lines. P_{G1-G5} means generators. P_{L1-L10} means loads. Discontinuous red lines represent normally open lines. Zone colors from Fig. 1 (i.e., orange zone for HIL 1 and blue zone for HIL 2). Grid's base characteristics from [40].

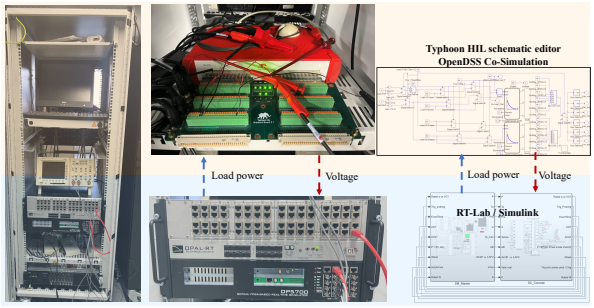

FIGURE 3. Experimental dual-HIL testbench. From left to right: board front, Typhoon HIL 402 (back) vs. OPAL-RT OP5700, and example signal exchange between models. Orange: power system side; blue: load side. Arrow colors indicate signal origin.

A. Parametric study

Firstly, a parametric study is conducted to theoretically evaluate the reliability of using (3) for DT creation. The study is performed by running the OpenDSS software [43] through the Python library opendssdirect [44]. After defining the grid operation setup (in this case study, adapted from [40]), the procedure is as follows: (i) update the consumed power at the selected node according to the unknown load profiles, time step, and probing signal (launched by controlled load); (ii) execute the power flow and store voltages and powers; (iii) repeat until the end of the simulation; and (iv) apply (3) to the collected data. By means of this procedure, numerous scenarios can be considered to analyze the DT performance.

In this work, (6) defines the unknown-load power (P_{unk}) at the same node as the controllable load. The expression, inspired by Fourier-type decompositions, is proposed as a flexible parametrized model to represent a wide range of distribution-side load behaviors, including those influenced by converter-interfaced devices with richer spectral content, within DT-oriented parametric analyses.

$$P_{\text{unk}}(t) = \sum_{p=1}^{n} \left[\frac{|P_{\text{unk}}|}{n} \cos\left(\frac{2\pi t}{\frac{Per_{\text{unk}}}{p}} + \frac{2\pi p}{n} \text{ sh} \right) + \frac{|P_{\text{unk}}|}{n} \right] \tag{6}$$

The Digital Twin is continuously updated to capture uncertainties from other time-varying consumptions. When

This article has been accepted for publication in IEEE Open Access Journal of Power and Energy. This is the author's version which has not been fully edited and content may change prior to final publication. Citation information: DOI 10.1109/OAJPE.2026.3666226

no information is available, (6) assumes the p^{th} load has the same amplitude as the remaining $n-p$ loads. "sh" is a Boolean variable that activates the angular shift between cosine functions. If $\text{sh}=1$, the loads are phase-shifted proportionally to their index p. The parameter Per_{unk} denotes the consumption period.

The controllable load employs a simplified version of (6) to generate the probing signal, neglecting additional loads, temporal shifts, and varying periods. Figure 4 presents the goodness of fit for 10,000 scenarios (combinations of 100 values of P_{unk} and Per_{unk}). The y-axis represents the ratio between the periods of the unknown and controllable loads, while the x-axis represents the ratio between their power amplitudes. Lighter colors, as shown in the color bar, correspond to a better fit (R^2). Red and green markers on the surface indicate cases with $R^2 \geq 0.9$ and $0.8 \leq R^2 < 0.9$, respectively.

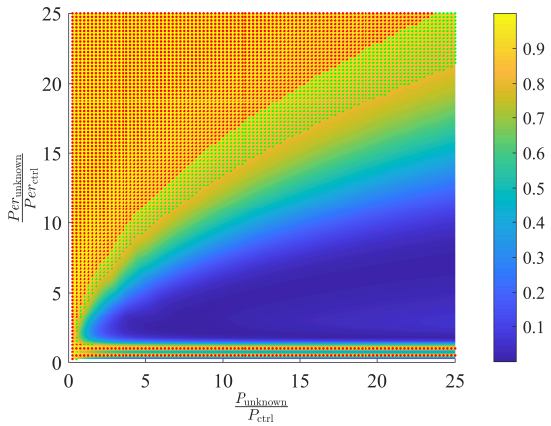

FIGURE 4. Goodness of fit (R^2) of (3) under different periods and power amplitudes of a single unknown load with non-varying period.

It can be observed that slower cumulative unknown loads yield better fits. Conversely, when the unknown load is significantly larger than the controllable load, the likelihood of a good fit decreases. As noted in Section III-A, the implemented LR considers only a single power. Consequently, if the voltage dynamics are sufficiently sensitive to the neglected terms, the fit provided by (3) may not accurately capture the system behavior. Figures 5 and 6 show the influence of the power factor of the connection-node and load unbalance, respectively, as disturbance terms. Under the same parametric conditions as in Fig. 4, both cases exhibit similar performance, with about 30% of the scenarios achieving $R^2 > 0.9$.

Depending on the grid under study, a single node may host multiple loads with diverse patterns and amplitudes. Since the proposed DT is intended to operate with any load, it is reasonable to consider a larger number of loads from the end-user perspective. Equation (6) can be extended to incorporate additional loads and thus generalize the results illustrated in Fig. 4. Figure 7 depicts the percentage of cases with $R^2 > 0.9$ as a function of the number of loads

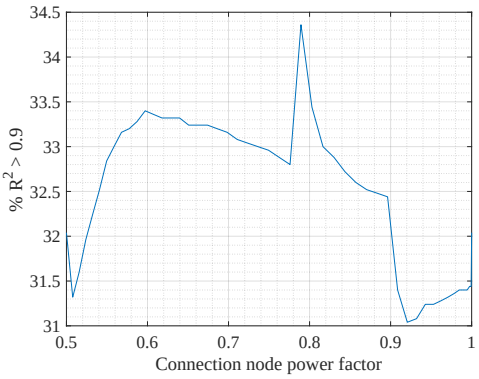

FIGURE 5. Influence of the global power factor in the load connection node over $R^2 > 0.9$ density.

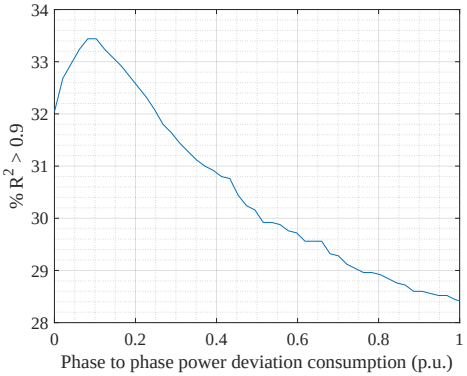

FIGURE 6. Influence of the power unbalance of the unknown load over $R^2 > 0.9$ density.

(up to 100 loads). Each point represents a set of simulated scenarios analogous to those in Fig. 4. Although no strictly monotonic relationship is observed, the overall trend is positive, suggesting that increasing the number of dispersed loads does not necessarily compromise the accuracy of the DT.

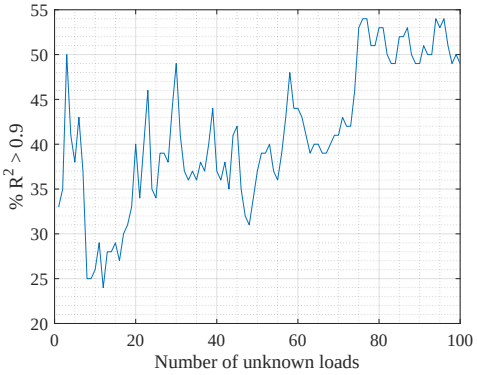

FIGURE 7. Influence of number of shifted and period-varying unknown loads over $R^2 > 0.9$ density.

B. Digital Twin real-time experimental validation

Once the theoretical feasibility of the DT creation is established, the methodology is evaluated under more realistic operating conditions, including analog signal processing, communication delays, high-frequency noise (e.g., switching effects, digital–analog conversion), computational load, and the accuracy limitations of numerical methods. These practical aspects are often neglected in purely theoretical studies. The framework illustrated in Fig. 1 is implemented without voltage control. In this case, in HIL 2, the dashed-arrow data flow predominates over the continuous arrow.

For a technically viable implementation relying on a reduced set of measurable signals, the motor shaft speed is employed to map setpoint power into setpoint speed. This is enabled by the well-known affinity laws [45]. In parallel with voltage and power measurements, the rotational speed is recorded, and the ratio $r_{\text{P-to-}\omega} = \frac{P_{\text{ctrl}}}{(\omega_{\text{mtr}})^3}$ is calculated to further obtain the setpoint speed as $(\omega_{\text{set}})^3 = \frac{P_{\text{set}}}{r_{\text{P-to-}\omega}}$. In this sense, both the probing signal and the voltage-control-based power setpoint are inherently constrained by the intrinsic dynamics and operational limits of the controllable load.

As detailed in Section IV-A, more than $1e^6$ ($[n]_{100\text{x}1}$, $[P_{\text{unk}}]_{100\text{x}1}$, and $[Per_{\text{unk}}]_{100\text{x}1}$) scenarios are simulated. Without aiming for completeness, only representative selected cases are presented. Validation of the DT creation methodology highlights potential regions of optimal operation. Figures 8, 9, and 10 depict the voltage behavior (blue), probing signal power (orange), and predicted power from the DT model (3) (green). Compared with Fig. 4, the three cases demonstrate $R^2 \geq 0.9$, particularly Figs. 8 and 9. The case in Fig. 10 instead falls within $0.8 \leq R^2 < 0.9$, showing the strongest influence of realistic conditions. The three DT-based power predictions accurately fit the real power. Additionally, it can be seen how the lowest fit (Fig. 10) provided slightly larger deviations. Overall, the trend indicates that higher probing signal frequencies enhance the goodness of fit. From a mathematical standpoint, faster probing signals effectively render other dynamics quasi-static. It is important to note that, for all cases shown, the probing signal produces a voltage deviation range below 4%. As illustrated in Fig. 8, the minimum observed deviation is approximately 1.3%.

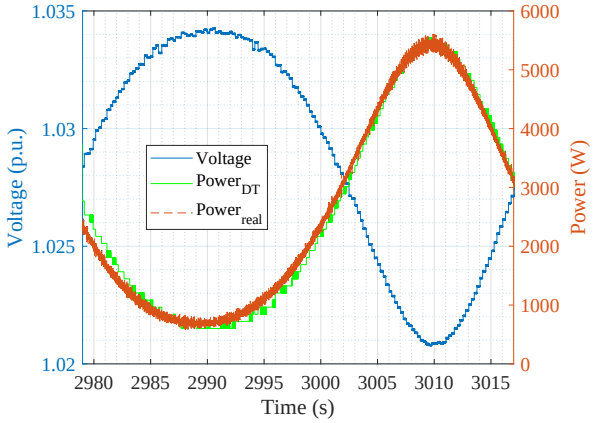

FIGURE 8. Online DT creation. The probing signal period and amplitude are 20 and 5 times smaller, respectively. Goodness of fit: $R^2 = 0.97$.

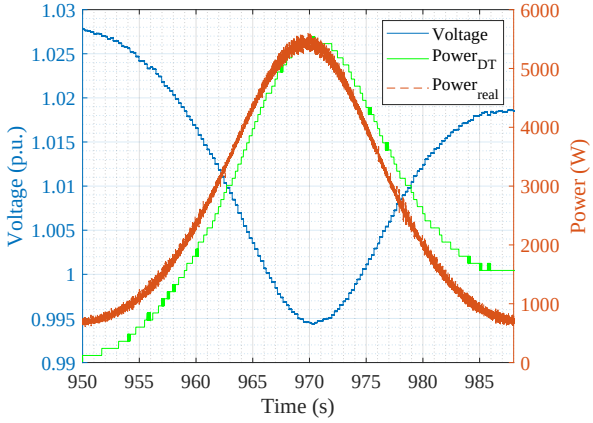

FIGURE 9. Online DT creation. The probing signal period and amplitude are 15 and 2 times smaller, respectively. Goodness of fit: $R^2 = 0.91$.

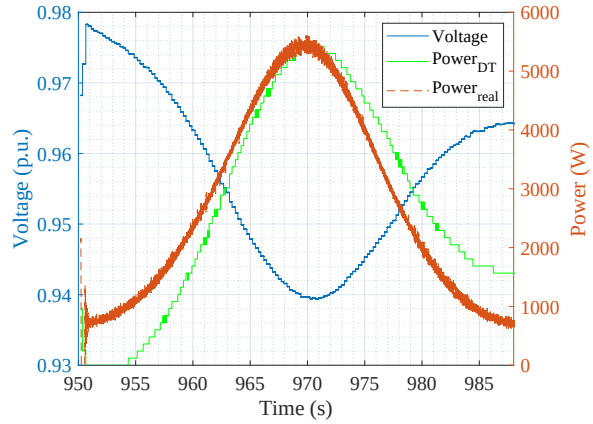

FIGURE 10. Online DT creation. The probing signal period and amplitude are 10 and 2 times smaller, respectively. Goodness of fit: $R^2 = 0.82$.

This article has been accepted for publication in IEEE Open Access Journal of Power and Energy. This is the author's version which has not been fully edited and content may change prior to final publication. Citation information: DOI 10.1109/OAJPE.2026.3666226

C. DT-enabled voltage support real-time demonstration

Once the DT creation methodology performs accurately in real-time, one possible use is to enable the controllable load to provide voltage control. As mentioned, the provision of this control aims to enable distributed load to contribute to the global enhancement of voltage performance, not to solve deviations themselves [18]. Therefore, the scenarios' conditions are set to clearly appreciate the contributions of non-extensive distributed loads.

Under a rated power penetration of 25% controllable load, power perturbations up to one-third of the controllable-load rating are considered. This penetration level is selected as a representative operating point for real-time validation, while the large-scale parametric study in Section IV-A already explores a wide range of penetration ratios and disturbance amplitudes. The voltage-control schemes in (5) are evaluated under the same admissible power range ($6e^2 \leq P_{\text{ctrl}},(W) \leq 6e^3$), where Mode E represents a grid-code-based droop control [8].

For assessing multiple asynchronous scenarios, with different initial conditions and exposed to different non-controllable conditions (e.g., delays and noise), the use of common statistics is proposed. Table 1 shows the maximum, minimum, and root mean square (RMS) voltage deviation (ΔV) of the ten different scenarios: five compared controls and two amplitudes of power perturbation (the extrema from 5/5 to 1/5 of maximum power amplitude considered).

At first glance, every DT-based voltage control performs better than a classic droop (Mode E). The smallest RMS ΔV is obtained by Mode B and the largest by Mode E, in both perturbation amplitude scenarios. Under the same perturbation, Mode B still provides the smallest maxima and minima. The DT-based droop control, Mode D, outperforms the classic droop control, Mode E, in almost any statistic (except Max ΔV at larger perturbation amplitude).

TABLE 1. Assessment of the voltage performance. Provision of voltage control according to the modes of (5) under different perturbation signal amplitudes.

Mode - $\lvert Pert_{\max}\rvert$	Max ΔV (V)	Min ΔV (V)	RMS ΔV (V)
A - 1/5	4.2867	3.8691	4.0661
B - 1/5	2.1051	0.7638	1.0088
C - 1/5	6.9180	1.1863	3.7675
D - 1/5	3.7245	0.8376	2.5399
E - 1/5	4.3129	3.8097	4.0718
A - 1	5.0345	3.0068	4.0390
B - 1	1.9560	-0.0384	1.2602
C - 1	7.9586	0.5698	3.6786
D - 1	6.7188	0.0823	2.6178
E - 1	4.9906	3.2149	4.0625

In terms of the selected statistics, Mode B performed the best among all scenarios. Figure 11 shows the voltage deviations under different perturbation power amplitude conditions, all during Mode B voltage control. This figure illustrates the impact of the perturbation power on the global voltage deviations.

As stated above, the scenarios are run asynchronously and sequentially without interruptions on the testbench of Fig. 3, accounting for continuous real-time deployment of the DT creation methodology and DT-based voltage control. This can be inferred by the time shifts among Fig. 11 signals.

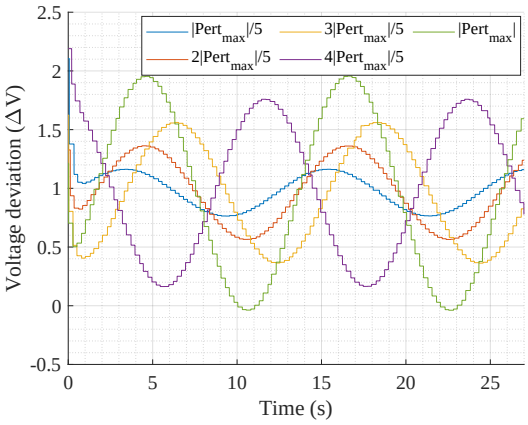

FIGURE 11. Mode B voltage deviations under different perturbation signal amplitudes. Data recorded in the Typhoon HIL 402.

Although the impact on thermal comfort has been analytically demonstrated in [14], prior studies on ancillary service provision through DTs have generally neglected this requirement during experimental validation [20]. Figure 12 illustrates the evolution of temperature deviation under voltage control. The deviation remains negligible and exhibits nearly identical values across scenarios. The minor discrepancies observed are attributed to the inherent behavior of individual heat gains, $\dot{Q}j$, and thermal exchanges between adjacent systems, $U\text{ji}A_{\text{ji}}$. These results indicate that even after five consecutive 25-second voltage control events, thermal comfort is expected to be preserved.

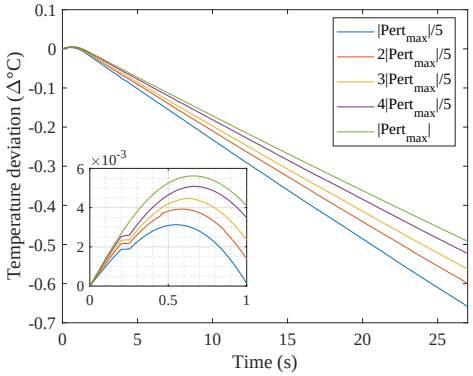

FIGURE 12. Mode B temperature deviation referred to the scenario initial value under different perturbation signal amplitudes during voltage control provision. Data recorded in the OPAL-RT OP5700.

V. CONCLUSION

The growing presence of converter-interfaced generation and loads introduces major challenges for modern power systems. This work extends the use of Digital Twins by enabling almost any load to support voltage control, even when grid information is limited or unavailable. A data-driven grid Digital Twin is proposed that relies only on one grid-voltage signal and the load's consumed power, allowing simple and low-cost deployment without additional hardware. The Digital Twin is obtained through a probing-signal-driven, one-input/one-output linear regression model that treats unmodeled dynamics as temporary noise, and is periodically relaunched to ensure continuous model updating.

To assess the proposal's reliability, three testing environments were used. First, a Python–OpenDSS setup enabled a large parametric study (over one million cases) to evaluate accuracy under varying load conditions. Second, a dual-HIL platform validated Digital Twin creation under real-time and analog I/O constraints. Third, the same setup was extended to test voltage control by generating the Digital Twin, computing a power setpoint from measured voltage, and applying it as a speed reference through the HVAC controllers.

The findings of the Digital Twin validation, implementation, and utilization can be summarized as follows:

- Using sinusoidal probing and unknown-load signals, highly accurate Digital Twins ($R^2 > 0.9$) are obtained when the probing is faster than the unknown-power variations.
- Across more than $1e^4$ combinations, over 30% achieved $R^2 > 0.9$, while including $R^2 > 0.8$ raised the coverage to approximately 80%, demonstrating robustness across diverse operating conditions.
- Increasing load heterogeneity does not reduce the likelihood of highly accurate Digital Twins; with 100 simultaneous loads, the probability of achieving $R^2 > 0.9$ rises to 50%.
- Dual-HIL experiments confirm that higher model complexity and technical realism do not hinder Digital Twin creation, with selected cases achieving $R^2 = 0.97, 0.91$, and 0.82, and with faster probing consistently yielding higher accuracy.
- Digital Twin-based voltage control (Modes A to Mode D) exhibited lower RMS ΔV than the classical droop reference (Mode E) across the considered scenarios. Under 20% perturbation amplitude, the reductions were 0.14%, 75.22%, 7.47%, and 37.62%; under full load, 0.58%, 68.98%, 9.45%, and 35.56%, respectively.

This work shows that a low-cost, data-driven Digital Twin can be accurately developed and effectively used to enhance voltage control from distributed loads, particularly converter-interfaced thermal loads. To our knowledge, it is among the first applications of Digital Twins to flexible loads. The results show that Digital Twins performance is chiefly limited by load characteristics, including relative size, controllability, and intrinsic dynamics.

A. FUTURE WORKS

Future research will include validating the methodology with high-resolution, real-world load profiles and extending the data-driven formulation to more complex load and control models and higher penetrations of converter-interfaced resources. The Digital Twin framework will be generalized to support multi-phase measurements, detailed unbalanced conditions, extensive reactive power effects, highly-distorted grids (e.g., due to converters' penetration), faults (including multiple types and durations), as well as topology changes or other operating conditions, that alter the grid's local sensitivity. Additional work will establish probing-signal constraints for safe operation of converter-interfaced loads and quantify latency, timing, and bandwidth effects for integration into controller design and hardware testing. Lastly, developing a coordinated framework for Digital Twin creation, updating, validation, and operation will facilitate the transition from HIL-based prototyping to practical field deployment.

Author Contributions

Author contributions according to Contributor Roles Taxonomy (CRediT): *Conceptualization:* J.A., A.L.; *Methodology:* J.A., A.L.; *Formal analysis:* J.A.; *Investigation:* J.A.; *Resources:* J.A., A.L.; *Data curation:* J.A.; *Writing - original draft:* J.A.; *Writing - review and editing:* J.A., A.L., Y.B., F.W., S.W., V.H.; *Visualization:* J.A.; *Supervision:* A.L., Y.B., F.W., S.W., V.H.; *Project administration:* A.L., Y.B., F.W., S.W., V.H.; *Funding acquisition:* A.L., Y.B., F.W., V.H.

REFERENCES

[1] IRENA, *Climate Action Support 2024*. Abu Dhabi: International Renewable Energy Agency, 2024.
[2] P. Denholm *et al.*, "The challenges of achieving a 100% renewable electricity system in the united states," *Joule*, vol. 5, pp. 1331–1352, 6 2021.
[3] J. Wachter, L. Gröll, and V. Hagenmeyer, "Survey of real-world grid incidents–opportunities, arising challenges and lessons learned for the future converter dominated power system," *IEEE Open Journal of Power Electronics*, vol. 5, pp. 50–69, 2024.
[4] J. Shair *et al.*, "Power system stability issues, classifications and research prospects in the context of high-penetration of renewables and power electronics," *Renewable and Sustainable Energy Reviews*, vol. 145, 7 2021.
[5] G. De Carne *et al.*, "The role of energy storage systems for a secure energy supply: A comprehensive review of system needs and technology solutions," *Electric Power Systems Research*, vol. 236, p. 110963, 2024.
[6] N. Hatziargyriou *et al.*, "Definition and classification of power system stability - revisited & extended," *IEEE Transactions on Power Systems*, vol. 36, pp. 3271–3281, 7 2021.
[7] W. Murray, M. Adonis, and A. Raji, "Voltage control in future electrical distribution networks," *Renewable and Sustainable Energy Reviews*, vol. 146, p. 111100, 2021.
[8] H. Sun *et al.*, "Review of challenges and research opportunities for voltage control in smart grids," *IEEE Transactions on Power Systems*, vol. 34, no. 4, pp. 2790–2801, 2019.
[9] F. Wald *et al.*, "Applications and services of solid-state transformers in active distribution networks—a critical review," *IEEE Transactions on Smart Grid*, vol. 16, no. 5, pp. 3615–3637, 2025.

[10] C. Li *et al.*, "A survey on the current state of demand response implementations: Models and approaches," *SIGENERGY Energy Inform. Rev.*, vol. 5, no. 1, p. 12–24, Aug. 2025.

[11] W. Du, L. Wang, and W. Luo, "Advancements and challenges in grid voltage control: A comprehensive review of intelligent technologies and future directions," in *2024 4th International Conference on Smart City and Green Energy (ICSCGE)*, 2024, pp. 252–256.

[12] Y. G. Werkie, G. N. Nyakoe, and C. W. Wekesa, "Power system voltage stability assessment and control strategies: State-of-the-art review," *Journal of Electrical and Computer Engineering*, vol. 2025, no. 1, p. 6667482, 2025.

[13] J. Araúz and S. Martinez, "Using the thermal inertia of trains for contributing to primary frequency control in grids with photovoltaic generation," in *2023 IEEE International Conference on Electrical Systems for Aircraft, Railway, Ship Propulsion and Road Vehicles & International Transportation Electrification Conference (ESARS-ITEC), Venice, Italy, 2023, pp. 1-6*. IEEE, 3 2023.

[14] ——, "Using the thermal inertia of trains for contributing to primary and supplementary frequency control in grids with high penetration of renewable generation," *IEEE ACCESS*, vol. 12, pp. 63 271–63 281, 5 2024.

[15] J. Araúz *et al.*, "Combined frequency control from trains thermal inertia: An assessment of frequency controllers interaction," *IEEE Open Journal of Power Electronics*, pp. 1–10, 3 2025.

[16] J. Araúz and S. Martinez, "Contribution of the thermal inertia of trains to the primary frequency control of electric power systems," *Sustainable Energy, Grids and Networks*, vol. 34, p. 100988, 6 2023.

[17] Y. Son *et al.*, "Hardware implementation and market impacts of grid-supportive functions in end-use loads," United States Department of Energy, Technical Report NREL/TP-5D00-85188, Mar 2023.

[18] J. Araúz and S. Martinez, "Use of the thermal inertia of trains for contributing to primary frequency control and inertia of electric power systems," *IEEE Access*, vol. 11, pp. 57 099–57 116, 5 2023.

[19] Z. Song *et al.*, "Digital twins for the future power system: An overview and a future perspective," *Sustainability*, vol. 15, no. 6, 2023.

[20] J. Araúz *et al.*, "A novel digital twin-based framework and methodology for enhancing the contribution of loads to frequency control," *IEEE Access*, vol. 13, pp. 128 475–128 491, 2025.

[21] Z. Dai *et al.*, "Efficient state estimation through rapid topological analysis based on spatiotemporal graph methodology," *IEEE Open Access Journal of Power and Energy*, vol. 11, pp. 396–409, 2024.

[22] S. Ebrahimi *et al.*, "Resilient space operations with digital twin for solar pv and storage," *IEEE Open Access Journal of Power and Energy*, vol. 11, pp. 624–636, 2024.

[23] T. P. Tran *et al.*, "Voltage control using optimization-based method in a digital twin," in *2024 IEEE 22nd Mediterranean Electrotechnical Conference (MELECON)*, 2024, pp. 138–143.

[24] Z. Wang *et al.*, "Voltage control of distribution network based on parallel control system," in *2023 IEEE 3rd International Conference on Digital Twins and Parallel Intelligence (DTPI)*, 2023, pp. 1–5.

[25] Y. Jung *et al.*, "Adaptive volt–var control in smart pv inverter for mitigating voltage unbalance at pcc using multiagent deep reinforcement learning," *Applied Sciences*, vol. 11, no. 19, 2021.

[26] S. Gupta *et al.*, "Deep learning for scalable optimal design of incremental volt/var control rules," *IEEE Control Systems Letters*, vol. 7, pp. 1957–1962, 2023.

[27] M. A. T. Mendoza *et al.*, "Digital twin adaptive remedial action scheme for preventing voltage collapse," *IEEE Journal of Emerging and Selected Topics in Industrial Electronics*, vol. 6, no. 2, pp. 523–535, 2025.

[28] D. A. Khan *et al.*, "Combined dr pricing and voltage control using reinforcement learning based multi-agents and load forecasting," *IEEE Access*, vol. 10, pp. 130 839–130 849, 2022.

[29] N. Mchirgui *et al.*, "The applications and challenges of digital twin technology in smart grids: A comprehensive review," *Applied Sciences*, vol. 14, no. 23, 2024.

[30] M. Jafari *et al.*, "A review on digital twin technology in smart grid, transportation system and smart city: Challenges and future," *IEEE Access*, vol. 11, pp. 17 471–17 484, 2023.

[31] Y. Gui *et al.*, "Voltage support with pv inverters in low-voltage distribution networks: An overview," *IEEE Journal of Emerging and Selected Topics in Power Electronics*, vol. 12, no. 2, pp. 1503–1522, 2024.

[32] W. H. Kersting, *Distribution System Modeling and Analysis*, 3rd ed. Taylor & Francis, 2012, p. 455.

[33] U. Kühnapfel and V. Hagenmeyer, *On the Art of Electric Power System Modelling and Simulation for Integrated Transmission-Distribution Analysis*. Springer Nature Switzerland, 2025, pp. 117–133.

[34] G. Casella and R. L. Berger, *Statistical Inference*, 2nd ed. Pacific Grove, CA, USA: Duxbury/Thomson Learning, 2002.

[35] N. Guruwacharya *et al.*, "Data-driven modeling of grid-forming inverter dynamics using power hardware-in-the-loop experimentation," *IEEE Access*, vol. 12, pp. 52 267–52 281, 2024.

[36] A. Arif *et al.*, "Load modeling—a review," *IEEE Transactions on Smart Grid*, vol. 9, no. 6, pp. 5986–5999, 2018.

[37] A. Labonne, "Méthodes et Outils pour la simulation et la validation expérimentale temps-réel des réseaux intelligents ou "Smart Grids"," Theses, Université Grenoble Alpes [2020-....], Nov. 2022.

[38] V. H. Nguyen *et al.*, *Hardware-in-the-Loop Assessment Methods*. Springer International Publishing, 2020, pp. 51–66.

[39] J. Markovic and S. Simic. (2024) Opendss & typhoon hil co-simulation. [Online]. Available: https://www.typhoon-hil.com/documentation/typhoon-hil-application-notes/References/opendss_power_flow_co_simulation.html

[40] M. C. Alvarez-Herault *et al.*, "An original smart-grids test bed to teach feeder automation functions in a distribution grid," *IEEE Transactions on Power Systems*, vol. 33, no. 1, pp. 373–385, 2018.

[41] A. Labonne *et al.*, "Distribution network," 2025. [Online]. Available: https://doi.org/10.57745/E25YTA

[42] TheMatworksInc. (2006) Space vector pwm vsi induction motor drive. [Online]. Available: https://www.mathworks.com/help/physmod/sps/examples/ac2-space-vector-pwm-vsi-induction-3hp-motor-drive.htm

[43] Electric Power Research Institute, "Opendss," https://www.epri.com/pages/sa/opendss, 2025, accessed: Sep. 24, 2025.

[44] D. Krishnamurthy, P. Meira, and D.-E. contributors, "Opendssdirect.py," https://pypi.org/project/OpenDSSDirect.py/, 2024, accessed: Sep. 24, 2025.

[45] R. Kent, "Services," in *Energy Management in Plastics Processing*, 3rd ed., R. Kent, Ed. Elsevier, 2018, pp. 105–210.

Jesús Araúz received the B.S. degree in Electromechanical Engineering from UTP, Panama, in 2020, and the M.S. degree in Electrical Engineering and the Ph.D. degree in Electrical and Electronic Engineering from the Universidad Politécnica de Madrid, Spain, in 2021 and 2024, respectively. His research interests include railway systems, building energy performance, renewable integration in low-inertia grids, demand response, and ancillary services in power systems.

Antoine Labonne received the M.S. degree in mechatronics from the University of Blaise Pascal, Aubiere, France, in 2005, and the Electrical Engineering Diploma from the Grenoble Institute of Technology, France. He is currently an Engineer with Grenoble INP and the G2Elab, where he obtained the Ph.D. degree in 2022. His research interests include interoperability and SCADA-as-a-service, cyber-physical energy systems validation, and hardware-in-the-loop for energy systems.

Yvon Besanger (Senior Member, IEEE) received the Ph.D. degree in electrical engineering from the Grenoble INP, in 1996. He is currently a Professor with the ENSE3, Engineers' School for Water, Energy and Environment Sciences, and the Grenoble Electrical Engineering Laboratory. His research interests include the distribution networks' operation and reliability, blackout prevention, power system security, and interoperability in smart grids.

Frederic Wurtz (Member, IEEE) received the Ph.D. degree in electrical engineering from the Grenoble Institute of Technology (Grenoble INP), France, in 1996. He is currently a CNRS Senior Researcher with the Grenoble Electrical Engineering Laboratory. His research interests include the design of electromagnetic devices and the system-level design of energy management for vehicles, buildings, and smart grids with an interdisciplinary approach.

Simon Waczowicz received the Ph.D. degree in mechanical engineering from KIT in 2018. Since then, he has headed the Research Platform Energy department at the IAI at KIT. His research interests include energy system design and operation, and time series analysis and forecasting.

Veit Hagenmeyer (Member, IEEE) received the Ph.D. degree from Université Paris XI, Paris, France, in 2002. He is currently a Professor of Energy Informatics with the Faculty of Computer Science, and the Director of the IAI at KIT. His research interests include modeling, optimization and control of sector-integrated energy systems.